Journal of Biomedical Optics

SPIEDigitalLibrary.org/jbo

Optical parametric oscillator-based photoacoustic detection of hydrogen cyanide for biomedical applications

Denis D. Arslanov
Maria P. P. Castro
Noortje A. Creemers
Anne H. Neerincx
Marius Spunei
Julien Mandon
Simona M. Cristescu
Peter Merkus
Frans J. M. Harren

SPIE

Optical parametric oscillator-based photoacoustic detection of hydrogen cyanide for biomedical applications

Denis D. Arslanov,[a] Maria P. P. Castro,[b] Noortje A. Creemers,[a,c] Anne H. Neerincx,[a,c] Marius Spunei,[a] Julien Mandon,[a] Simona M. Cristescu,[a] Peter Merkus,[c] and Frans J. M. Harren[a]
[a]Radboud University Nijmegen, Life Science Trace Gas Research Group, Molecular and Laser Physics, Institute for Molecules and Materials, Nijmegen, The Netherlands
[b]Universidade Estadual do Norte Fluminense Darcy Ribeiro, Centro de Ciência e Tecnologia, Laboratorio de Ciências Fisicas, Campos, Brazil
[c]Radboud University Nijmegen Medical Centre, Department of Pediatrics, Nijmegen, The Netherlands

Abstract. A versatile, continuous wave, optical parametric oscillator is used in combination with photoacoustic spectroscopy for long-term trace gas experiments of volatile compounds emitted by biological samples. The optical parametric oscillator-based spectrometer (wavelength near 3 μm, 8-MHz linewidth, output power ~1 W) is successfully tested for the detection of hydrogen cyanide (HCN) emission from clover leaves, and *Pseudomonas* bacteria; in addition, the presence of HCN in exhaled human breath is measured. For specific experiments, the spectrometer is operated continuously up to 10 days and has a detection limit of 0.4 parts-per-billion volume of HCN in air over 10 s, using the P8 rotational line in the ν_3 vibrational band of HCN at 3287.25 cm^{-1}. This results in an overall sensitivity of the system of 2.5×10^{-9} cm^{-1} $Hz^{-1/2}$. [DOI: 10.1117/1.JBO.18.10.107002]

Keywords: hydrogen cyanide; laser-based detector; photoacoustic spectroscopy; optical parametric oscillator; gas sampling; *Pseudomonas* bacteria.

Paper 130426RR received Jun. 21, 2013; revised manuscript received Sep. 4, 2013; accepted for publication Sep. 6, 2013; published online Oct. 2, 2013.

1 Introduction

Hydrogen cyanide (HCN) is a volatile compound that can be found both in the liquid and gas phase; it is highly toxic and has a bitter—almond-like—odor. It is used in a number of industrial production processes, such as for adiponitrile $[(CH_2)_4(CN)_2]$ production (for nylon), methyl methacrylate, and pharmaceuticals.[1] HCN is also produced in other industrial activities such as electroplating, cleaning processes, and metallurgy. Due to its toxicity, an acute lethal dose of HCN, in $mg\,kg^{-1}$ body weight for humans 0.5 to 3.5 has been identified;[2,3] the exposure limit value considered to be lethal for humans is 200 part-per-million volume (ppmv) for 30 min and 600 to 700 ppmv for 5 min.[4] On the other hand, small amounts of HCN can be found in the human body due to endogenous biological processes; it may originate from endogenous production, bacteria, or ingestion of food containing HCN.[1]

In plant tissue, HCN can be produced as a result of hydrolysis of cyanogenic compounds, but also through the biosynthesis of the plant hormone ethylene.[5] Peiser et al. were the first to demonstrate that cyanide is a coproduct of ethylene biosynthesis.[6] It is estimated that >3000 plant species are able to produce HCN. The mechanism of HCN production in most species is by degradation of cyanogenic glycosides.[7] When the tissue is damaged the plant is able to synthesize these precursors of HCN. The cyanogenic glycosides will produce, among others, sugars, fatty acids, aldehydes, and HCN when they are hydrolyzed by enzymes. Several cyanogenic plants are edible, such as clover and apple;[8,9] however, the effect will only be toxic if ingested in large quantities from certain plant parts, such as seeds. In plant tissue, HCN amounts >20 mg/100 g are considered as a high risk.

HCN can also be produced in substantial amounts by bacteria.[10] From a medical point of view, this topic is almost not explored, but can be of high significance. Here, we will relate HCN production to *Pseudomonas aeruginosa* bacteria. These bacteria are dangerous for immune-compromised patients.[11] Infections with these bacteria are of particular significance in cystic fibrosis (CF) patients, due to their association with an increased morbidity and mortality.[12,13] CF itself is the most common, fatal genetic disease affecting Caucasians,[14] and is caused by a mutation in the gene coding for the CF transmembrane conductance regulator, a chloride channel.[14,15] Due to this mutation, the chloride efflux is impaired, which results in viscous, water deficient mucus in the airways, impaired mucociliary clearance, and an inability to effectively defend the airways from infections.[16,17] As a result, bacterial colonization and chronic airway infection mainly characterize the pathogenesis of CF lung disease.[18] It is, therefore, important to detect bacterial infections in the airways as early as possible.[19] However, current diagnostic techniques lack sensitivity (cough swab), are very invasive (Broncho Alveolar Lavage, BAL), and commonly miss early infections, especially in young children.

A sensitive and specific, noninvasive method for the diagnosis of *P. aeruginosa* infection would be extremely useful in medical sciences. An attractive, but hardly explored, avenue for noninvasive and fast medical diagnostics is a breath analysis. HCN is highly volatile and seems to be a promising indicator for *P. aeruginosa* infections. A recent study showed that HCN concentrations in the breath of *P. aeruginosa* colonized patients

Address all correspondence to: Frans J. M. Harren, Radboud University Nijmegen, Life Science Trace Gas Research Group, Molecular and Laser Physics, Institute for Molecules and Materials, Nijmegen, The Netherlands. Tel: +31-24-3652128; E-mail: F.Harren@science.ru.nl

0091-3286/2013/$25.00 © 2013 SPIE

are higher as compared to noninfected persons,[20] but these results remain inconsistent and inconclusive.[21,22] In the search for a noninvasive diagnostic biomarker for *P. aeruginosa* infections, HCN production should be quantified and investigated to a larger extent.

There is an increasing interest in the development of sensitive and selective methods to detect HCN.[20,23,24] Several studies have been conducted with different types of matrices, such as water, soil, air, exhaled breath, and food.[25–29] A large number of different methods have been used to monitor HCN: colorimetry and spectrophotometry,[30,31] optical detection following capillary electrophoresis,[32,33] fluorometry,[34] chemiluminescence,[35] potentiometry and amperometry,[36,37] mass spectrometry and gas chromatography,[38] as well as near-infrared cavity ring-down spectroscopy.[2,24] Most of these methods are complex and involve a large amount of manipulations of samples or the use of solvents. Furthermore, a number of these methods feature a slow response time (in the order of minutes) and hardly any continuous gas monitoring over days or weeks is performed. In most cases, the detection limit is in the ppmv mixing range, which is not sufficient to perform trace emission experiments on small amounts of biological samples. Thus, the development of more sensitive methods, to measure parts-per-billion volume (ppbv) level of HCN, appears to be very relevant.

Laser-based spectroscopic techniques can overcome most of the drawbacks of the conventional methods. They have the advantage of a high sensitivity, good selectivity, and wide-dynamic range. A high sensitivity is important to detect low trace gas concentrations and it is essential to identify the gas in a multicomponent gas mixture. In addition, a wide-dynamic range is required to monitor a wide range of concentrations for numerous gas components using the same instrument. Here, we use a continuous wave optical parametric oscillator (OPO) combined with the sensitive photoacoustic detection to achieve the required sensitivity and selectivity for the detection of HCN at the low part-per-billion volume range.

Nowadays, midinfrared singly resonant optical parametric oscillators (SROs) are considered as the most useful configurations for such sensitive gas sensing, due to their high power (Watt level), wide-tuning range, and ease of tenability.[39–41] Also, they can be as simple and compact as any basic linear OPO cavity, and displays low sensitivity to mechanical vibrations.[42] Among other laser spectroscopic methods, photoacoustic spectroscopy (PAS) serves as a very sensitive, efficient, easy, and robust method.[43–45] However, it cannot be easily used at sub-second time scales, which limits its use for fast detection such as is needed for real-time breath analysis.[46] Nevertheless, due to the above-mentioned advantages, it is preferably used in long-term experiments. In addition, PAS is relatively cheap and can be used at a very wide-wavelength range which is limited only by the transmittance of the PA window materials. In contrast to optical cavity enhanced approaches, such as cavity ring down or cavity enhanced spectroscopy[47,48] in which the wavelength dependence of the highly reflective mirror coatings limits the spectral coverage of the system. Combining OPOs with PAS has another important advantage. Photoacoustics utilize the high power of the infrared OPO, resulting in high sensitivity for the trace gas detection, since the generation of the photoacoustic signal is proportional with the laser power.[41] In the midinfrared wavelength region, many gases have strong fingerprint absorption spectra and each molecular gas has its own uniquely recognizable absorption spectrum that makes OPO-based absorption spectroscopy an excellent method for the selective detection of volatile organic compounds in complex gas mixtures. OPO-based PAS was described earlier for sensitive trace gas measurements,[49–52] however, it has not been previously used for the detection of HCN in biomedical applications.

Here, we present a study on HCN in different matrices. First, HCN emissions from clover leaves are used to verify the potential of the method concerning sensitivity, selectivity, and detection limits. After that, we present HCN presence in the exhaled breath. Finally, its emission from *P. aeruginosa* bacteria during their growth over a period of 13 days is presented. As such, the long-term stability of the setup was tested.

2 Experimental Setup

A 1064-nm distributed Bragg reflector (DBR) diode laser (EM4, Bedford, Massachusetts, USA) in a 14-pin butterfly package design is used as a seed source for the fiber amplifier (see Fig. 1). The laser has a linewidth of 8 MHz and is, therefore, a suitable source for Doppler-broadened spectroscopy of molecular gases. The laser has long-term stability better than 50 MHz over 4.5 h ($I = 250$ mA, operating temperature 25° C), which was measured using a Bristol 621A wavemeter (see Fig. 2), This stability accuracy was limited by the wavemeter. The compact laser diode driver (Multiwave, San Jose, California, USA) was modified to ensure faster wavelength scanning by changing the laser operating temperature. The temperature scans were performed by applying a saw-tooth current ramp on the thermo-electrical cooling of the laser. The maximum scanning range was set from 15 to 25°C to comply with the guaranteed technical specifications of the laser. Under these conditions, the maximum scanning wavelength range without any mode hops was between 9386.9 and 9391.6 cm^{-1} (see Fig. 3). Due to the laser temperature induced scanning and to the relatively slow response of the photoacoustic effect in the detection cell, a single laser scan over this wavelength range took 10 s, which cannot compete with the fast scanning speeds for similar DBR lasers used as pump sources for OPOs (Ref. 46). Nevertheless, faster scans were possible in the current configuration using a shorter-wavelength range. We recorded 1 cm^{-1}/s scanning speeds at 9390 cm^{-1}, and 0.5 cm^{-1} scanning range in 0.1 s. The scans were recorded

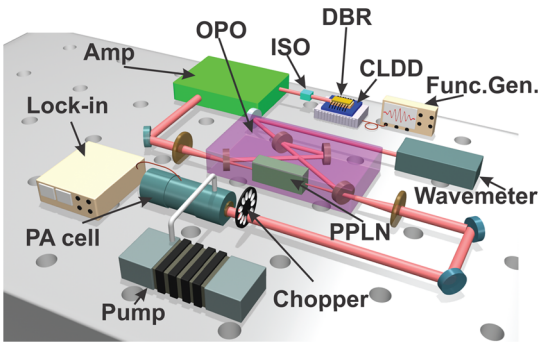

Fig. 1 Experimental setup of the optical parametric oscillator (OPO)-based photoacoustic detector for biomedical applications: DBR, 1064 nm distributed Bragg reflector laser; CLDD, compact laser diode driver; Func.Gen., function generator to drive CLDD; ISO, 30 dB optical isolator at 1064 nm; Amp, fiber amplifier; OPO, singly resonant optical parametric oscillator; PPLN, periodically polled lithium niobate crystal; PA cell, photoacoustic cell with Silcosteel coating.

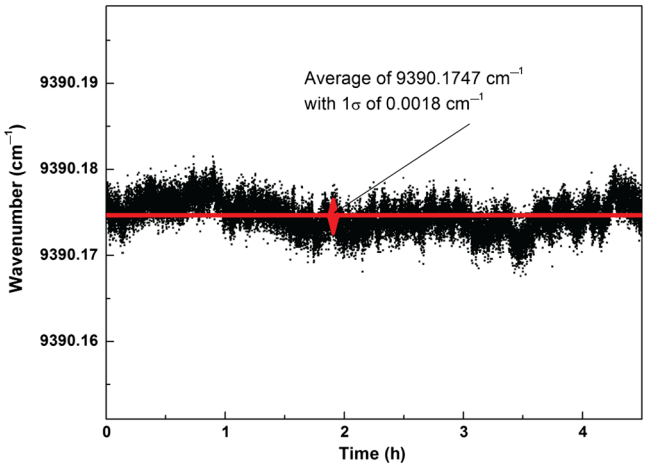

Fig. 2 Long-term frequency stability of the DBR seed laser at a constant current of 250 mA and a constant temperature of 25°C, which was <50 MHz (0.0018 cm^{-1}) over 4.5 h.

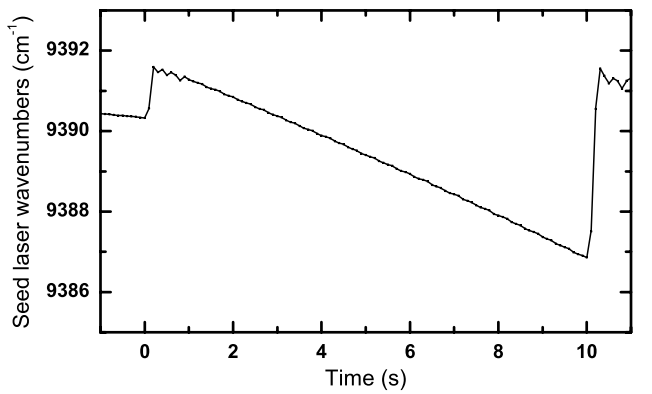

Fig. 3 Maximum wavelength mode-hop-free scans of the seed DBR laser up to 4.7 cm^{-1} at around 9390 cm^{-1} recorded in 10 s.

by the detection of a fringe pattern using a transmission of the laser light through a 2.54-cm long Germanium etalon (FSR = 1.48 GHz). The maximum output power of the DBR laser is 150 mW. In order to pump our SRO, with a pump threshold of 1.5 to 3.5 W (Ref. 52), we amplified the laser power with a fiber amplifier unit (Nufern, Model NUA-1064-PD-0010-C1). This amplifier has two amplification stages to allow a changing output power range from 0.8 to 12 W. To prevent feedback in our DBR laser an additional isolator (Thorlabs, Model 10-J-1064APC, 30 dB) was used.

The OPO unit itself is similar to the one described elsewhere.[40] Four mirrors, of which two plano-concave with radii of curvature of 20 cm and two plane mirrors, were used in a bowtie ring cavity configuration. The mirrors (diameter 25 mm, thickness 6.3 mm, QTF, USA) are highly reflective for the signal beam (~99.9% at 1450 to 1700 nm), highly transparent for the pump (~10% at 1062 to 1085 nm), and idler beam (~10% at 2.9 to 4.0 μm). The periodically poled lithium niobate crystal with 5% MgO doping (PP-MgO-LN) had seven periods with a periodicity ranging from 28.5 to 31.5 μm, with end facets at 90 deg /89 deg (HC Photonics, Hsinchu, Taiwan). The PPLN crystal was placed inside an oven capable of maintaining temperatures from 20 up to 200°C and the oven was controlled by a temperature controller (Thorlabs, Munich, Germany, Model TC200). The complete OPO cavity, including PPLN oven, was placed inside an aluminum housing, which was thermally stabilized at 30°C using a thermal bath (Tamson Holland) to maintain long-term (over days) wavelength and power stability.

The photoacoustic cell contained an open acoustical resonator (length 10 cm, diameter 5 mm) with two adjacent buffer volumes with a larger diameter.[49,50] As such, an acoustical standing wave in the open resonator is generated at a frequency of 1610 Hz with a Q-value of ~25. The aluminum cell was coated with a Silcosteel coating to reduce adsorption of polar gases and chemical reactions of gases on the cell wall material. The laser beam was modulated with a mechanical chopper to generate the acoustic effect, the enhanced photoacoustic signal was fed into a lock-in amplifier (dual phase, Model 7220, EG&G Instruments, Salem, Massachusetts).

To measure HCN, we used the wavelength region around 3287 cm^{-1} (Fig. 4). When measuring biological samples such as plants, seeds, bacteria, or human breath, attention has to be paid to interfering gases such as water and CO_2. As a result, only a limited number of transitions in the ν_3 band of the HCN can be selected. To estimate the interference of HCN absorption lines with water and CO_2 absorption lines, we calculated the ratio between the absorption coefficient, per 1 cm path length, of 10 ppbv of HCN and the sum of absorption coefficients of 1% water and 5% CO_2 based on HITRAN database[53] [see Fig. 4(a)]. This ratio helped to determine the best spectral regions for the detecting of HCN from biological samples. It plays a role of a first step of an analysis to limit the wavelength choice. The full analysis requires consideration of a few other factors, such as interfering gases in a gas mixture, concentrations of compounds, pressure, absolute intensity of a particular absorption line, availability of a laser source, etc. A few of those spectral regions are plotted in Fig. 4(b)–4(d). The P8 transition in the ν_3 band of HCN, at 3287.247603 cm^{-1} (Ref. 53), was found to be the best for our biological experiments. Although this HCN transition does not show the best ratio [Fig. 4(a)], it was chosen because it has less interference with CO_2 as compared to the transition at 3331.5 cm^{-1} [Fig. 4(d), P25 transition in the ν_3 band] and it has a stronger absorption than that at 3268.0 cm^{-1} [Fig. 4(b), P14 transition in the ν_3 band].

To perform a proper biological sampling, we had to overcome several complications to enable stable and reliable long-term measurements on HCN emissions. First, it is important to avoid any metal parts in the gas flow system from the biological sample to the photoacoustic detection cell; wall absorption by HCN on metal parts significantly reduced an initial gas mixing concentration and increased the response time of the gas flow system. For example, initially we had a metallic mass flow controller in the gas flow system. As a result, we observed an HCN response time of the gas flow system of many hours instead of seconds for nonpolar gases. This was demonstrated by applying a 1 ppmv calibrated HCN mixture in nitrogen into the system (Fig. 5); a 90% value was reached after 20 h. When we replaced all the gas sampling lines and gas connectors with Teflon lines and connectors (Polyfluor Plastics, The Netherlands) and Teflon valves (Valco valves, Bester BV, The Netherlands) the 90% response time became 5 min (flow rate of 2 L/h, volume of the system of 10 ml). For inert gases, the 90% response time will be 20 s. Furthermore, we replaced the pressure reduction valve of the high-pressure bottle containing the calibrated HCN mixture by a specially coated reduction valve. Second, we tried to de-humidify the sample gas using Nafion tubing. However, we observed gigantic losses

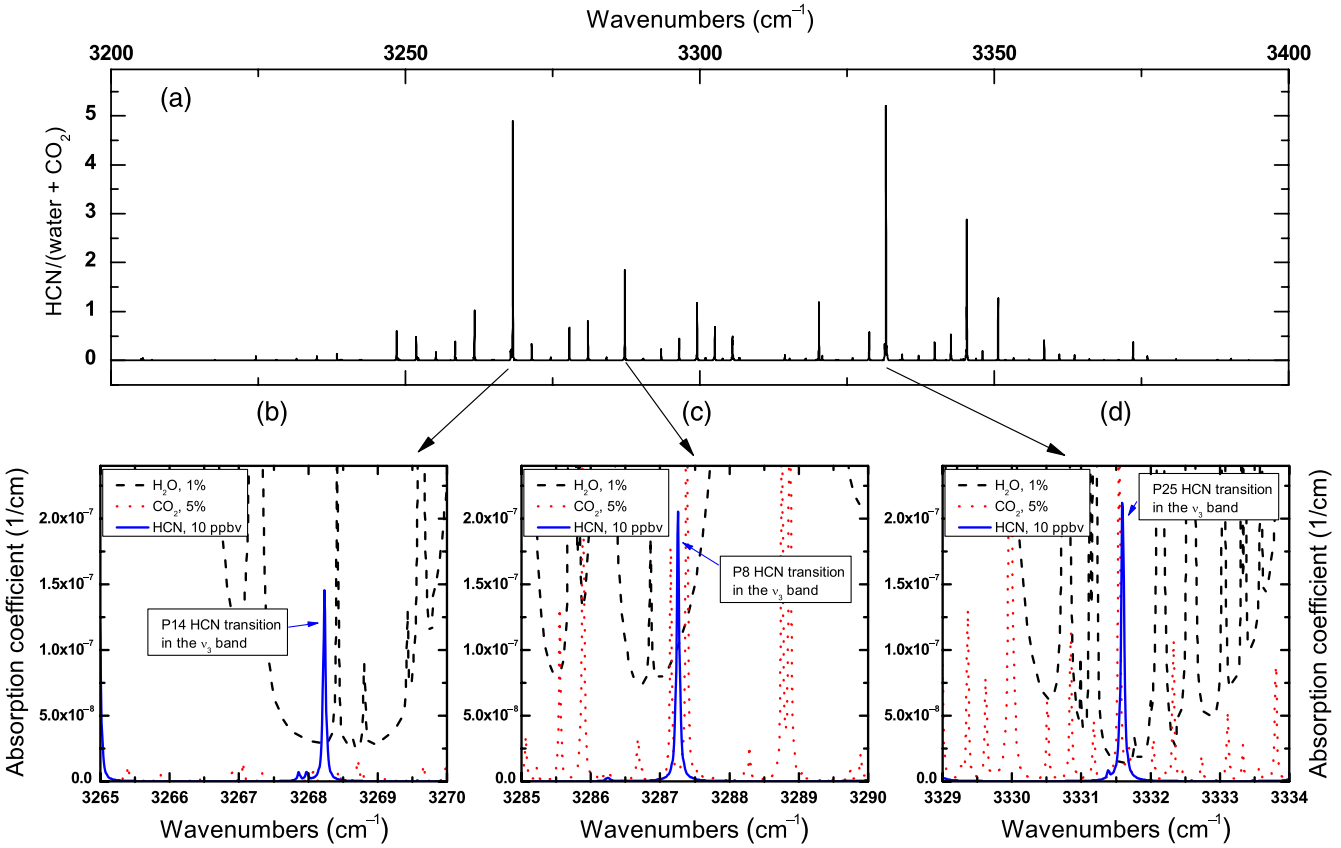

Fig. 4 (a) Ratio between 10 ppbv of HCN and a sum of 1% of water and 5% of CO_2 for a pressure of 200 mbar in the wavelength range of 3200 to 3400 cm^{-1} based on HITRAN database (Ref. 53); (b)–(d) Simulated spectra [using HITRAN database (Ref. 53)] at a pressure inside the photoacoustic cell of 200 mbar for 1% of water (black-dashed line), 5% of CO_2 (red-dotted line), and 10 ppbv of HCN (blue solid line) for the wavelength ranges: (b) 3265 to 3270 cm^{-1}, (c) 3285 to 3290 cm^{-1}, (d) 3329 to 3334 cm^{-1}. Arrows connecting the figures related to the wavelength regions for the ratio calculation (a) with simulated spectra (b), (c), and (d).

of HCN concentration in the gas flow, which is in contrast to the research described elsewhere.[2] The reason for this could be that we use a flow rate of 2 to 5 L/h, while elsewhere they used 30 L/h.[2] Therefore, we did not incorporate Nafion tubing in our sampling system. High water concentrations affect our HCN measurements in several ways. Water adds a nonlinear background on the top of the HCN absorption line (see Fig. 4).

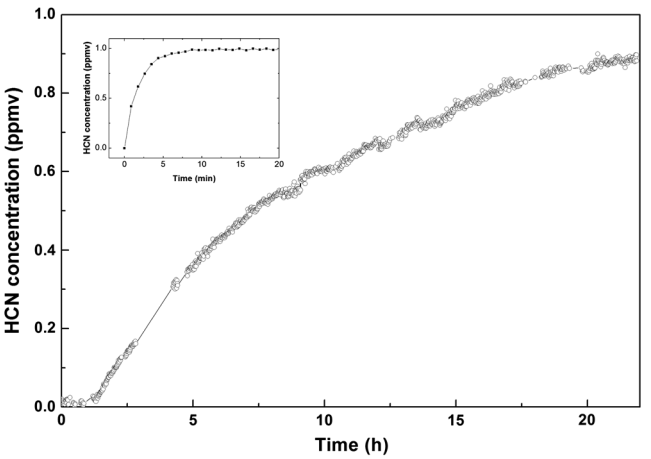

Fig. 5 Response time of 1 ppmv of HCN from the calibration mixture cylinder when using a noncoated reduction valve. A 90% value (0.9 ppmv) is reached after 20 h. Figure insertion shows the response time of 5 min of optimized system.

This is important because the water concentration will change over days when analyzing biological samples. In addition, due to the initial 100% relative humidity (RH) at 37°C (needed for the bacterial experiments) water vapor will condense inside sampling tubes at a lower room temperature, which will lead to the partial, or full, blocking of the gas flow system by water droplets.

These effects were eliminated by choosing the HCN absorption line at 3287 cm^{-1} that has a reduced spectroscopic interference with water lines, by lowering the pressure inside the photoacoustic cell (to 400 mbar), increasing the spectral resolution by reducing the pressure broadening, and by placing a cold trap (10°C) in the sampling flow from the sampling cuvettes to the photoacoustic cell thereby reducing the RH in the sampling flow below its dew point. A control experiment was carried out to ensure that the cold trap did not affect the measurements by trapping HCN.

3 Results and Discussion

The linear response of the system was tested by dynamically diluting a calibrated mixture of 5 ppmv HCN in N_2 (5 ppmv $\pm$ 5%, 10 l cylinder; Linde, The Netherlands) with pure N_2 in a concentration range from 1 ppmv to 100 ppbv (Fig. 6); an R^2 value of 0.999 was achieved. A calibration (Fig. 6) that is linear over the entire measurement range (from 100 to 1000 ppbv) allows determining the detection limit from standard deviations at a low concentration.[54] In addition, a detection limit of 0.40 ± 0.03 ppbv for HCN was

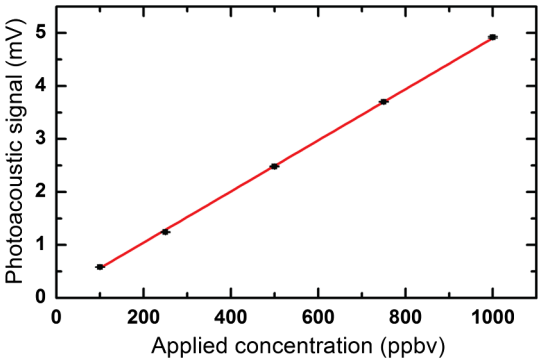

Fig. 6 HCN calibration measurements. Experimental points are the photoacoustic signal of five concentrations applied into the system. A detection limit of 0.40 ± 0.03 ppbv was achieved.

achieved in 10 s (at 3287.25 cm^{-1}). The detection limit was calculated for a signal-to-noise ratio = 1.

The HCN concentration values were calculated using a Curve Fitting Express application in the LabView environment. The Curve Fitting Express model displays the data of a signal function (a spectrum of a mixture of gases emitted by the sample with an unknown HCN concentration) against a location function (a spectrum with a known HCN concentration). The slope of a linear fit between the functions determines the HCN concentration.

3.1 *HCN Measurements from White Clover Leaves*

To demonstrate HCN emission from cyanogenic plants, 10 white clover leaves (*Trifolium repens*, total fresh weight of 0.313 g) were collected from the greenhouse of Radboud University. A spectrum of HCN containing gaseous mixture from clover leaves is shown in Fig. 7. Leaves were cut into 2-mm wide pieces and placed into a small glass cuvette with a gas inlet and outlet flow. A second identical cuvette served as a blank experiment for background measurements. A carrier gas flow, a mixture of 21% of O_2 in nitrogen, was used from a high pressure cylinder, while the pressure was reduced by a reduction valve and controlled with a mass flow controller (Brooks Instruments, The Netherlands). As such, a constant flow rate of 5 L/h was maintained over the leaves for days. The air flow speed was set just a bit higher than the pump speed of the vacuum pump to prevent under-pressure inside the cuvettes. Also, there were small overpressure outlets placed in-between sampling cuvettes and needle valve. The Teflon needle valve before the PA cell was set such that the pressure in the PA cell was reduced. Under such conditions, atmospheric pressure was kept inside the measuring cuvettes. To maintain a constant flow over the biological sample, electrically controlled three-way Teflon valves (MTV-3-N1/4UG Takasago, Japan) were used to either flow the sample gas into the photoacoustic cell or flow into an exhaust when the other blank cell is sampled. In such a way, identical flows and pressure conditions are maintained inside the sampling cuvettes during the whole experiment regardless of which cuvette is measured. Figure 8 shows the sampling setup and results for the clover leaves emission.

Initially, the photoacoustic cell was connected to the blank cuvette to measure background levels. Meanwhile, the damaged clover leaves were placed inside the sampling cuvette and the system was switched to the cuvette containing the clover. The HCN emission profile was monitored for 20 h and was

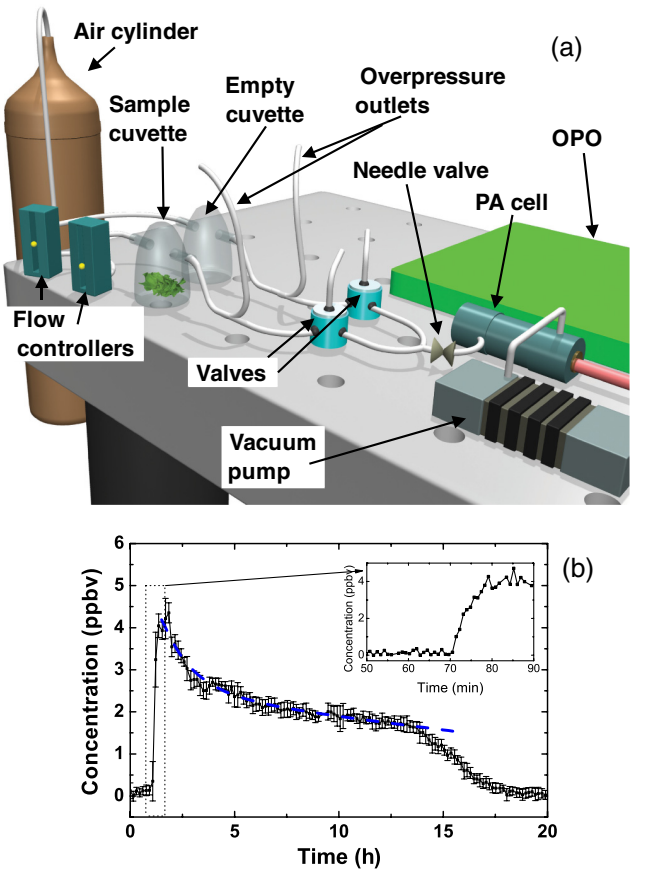

Fig. 7 Spectrum of HCN containing gaseous mixture from clover leaves recorded. The spectrum recorded shows the HCN peak at near 3287.25 cm^{-1} together with a water peak at near 3286.75 cm^{-1}. Vertical scale is in signal from the lock-in amplifier normalized per optical laser power.

stopped due to the dehydration of the clover leaves [Fig. 8(b)]. The inset of Fig. 8(b) shows the fast increase of HCN concentration from 0 level up to 4 ppbv within <10 min. The HCN decay curve, due to the cutting of the leaves between 1 and 12 h, is fitted exponentially and shows a decay time of 15.7 ± 0.8 h. After that, the HCN concentration dropped significantly faster to a 0 level from 12 to 18 h. This effect was found highly repeatable for various experiments and a reasonable explanation for this is dehydration of the leaves.

3.2 *HCN from Human Breath*

Breath analysis is a strongly growing field of research over the last decade. It is noninvasive, easy, safe, fast, and does not require a specific sample preparation, including laser-based breath analysis.[46,48,55] Here, we were not able to carry out real-time breath analysis as described elsewhere[46] due to the relatively slow photoacoustic response, but we performed the off-line breath analysis. Tedlar gas sampling bags (1 L Tedlar bags with 2 inlets/outlets) were used to collect and store human breath samples. A diaphragm membrane vacuum pump (MVP 015-4, Pfeiffer Vacuum, Germany) with a restriction valve was used to deliver a breath sample from a Tedlar bag into the photoacoustic cell for analysis. Here, the pressure inside the photoacoustic cell was set at 500 mbar. A valve system was used to switch between the bags. Figure 9 depicts the results of

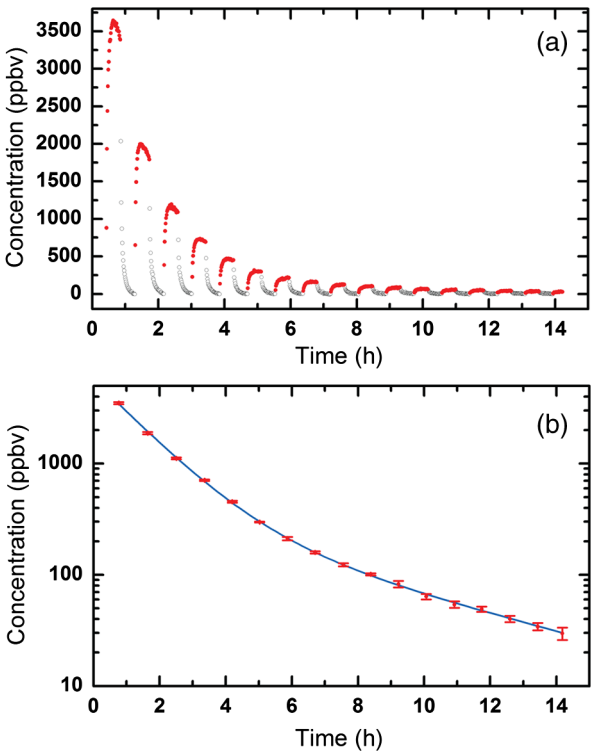

Fig. 8 (a) Artistic impression of the experimental scheme for the HCN detection from clover leaves: air cylinder, high pressure cylinder of synthetic air; flow controllers, mechanical mass flow controllers; sample cuvette, glass cuvette with the sample to analyze; empty cuvette, empty glass cuvette for reference comparison; overpressure outlets, outlets to prevent overpressure inside the cuvettes; needle valve, Teflon needle valve to reduce the pressure inside the PA cell; valves, diaphragm isolated three-way valves; OPO, continuous wave optical parametric oscillator; PA cell, photoacoustic cell with Silcosteel coating; vacuum pump, diaphragm membrane vacuum pump. (b) Concentration dynamics of HCN emitted from 10 cut clover leaves (fresh weight 313 mg). Blue-dashed line represents an exponential fit with value $t = (15.7 \pm 0.8)$ h. The insertion is a zoomed-in area of the dotted rectangle and it shows the response time of the system of few minutes. HCN dropped starting from 12 h reaching 0 level at 18 h due to the dehydration of leaves.

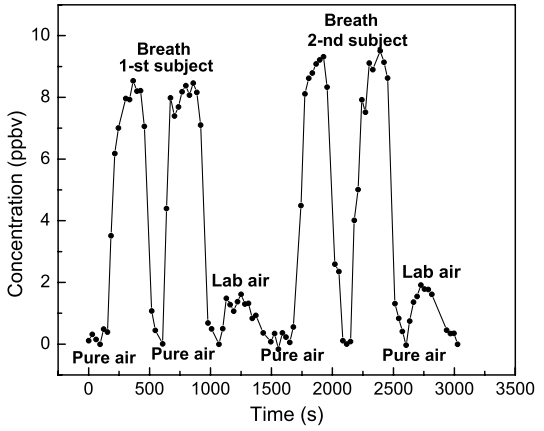

Fig. 9 HCN concentration from exhaled breath of two subjects repeated twice for every person. HCN value of about 1.5 ppbv was measured in the laboratory air and 0 HCN level from the synthetic air.

HCN measurements of clean air, HCN in the laboratory air at the time of measurements, and HCN in the breath of two volunteers (each 2 times sampled). The laboratory air contained 1.5 ppbv HCN while clean air did not show any presence of HCN. Both volunteers had an HCN concentration between 8 and 9 ppbv. The experiment also shows reproducibility when analyzing the breath of the same person. Our results are in agreement with the data obtained by Stamyr et al.[24]

3.3 *Detection of HCN Produced by Pseudomonas Bacteria*

Pseudomonas bacteria (ATCC 10145, obtained from Oxoid BV, The Netherlands) were cultured in liquid brain–heart infusion (BHI) broth and medium (Mediaproducts BV, The Netherlands) and incubated at 37°C, while constantly shaking at 70 rpm on an orbital shaker (Sanyo, Osaka, Japan). A

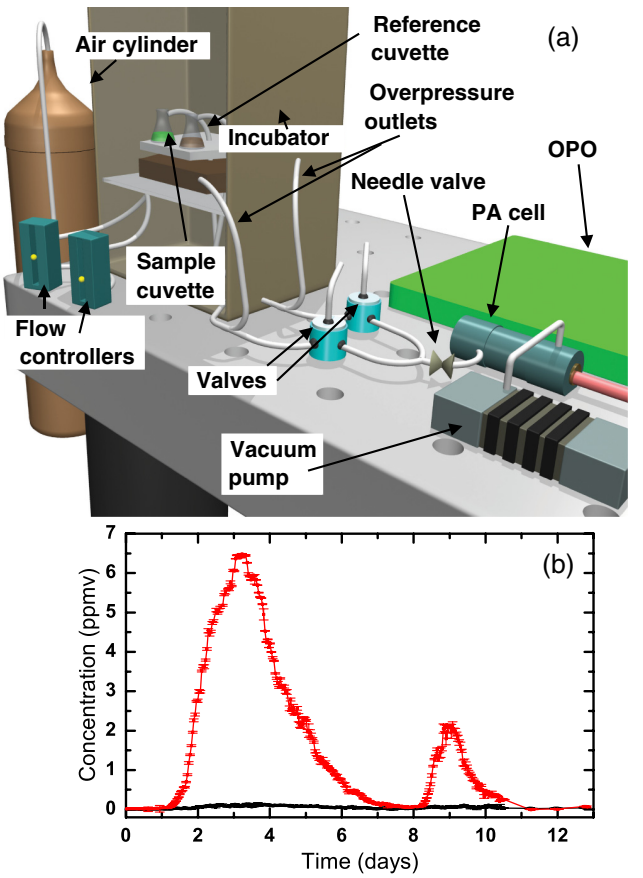

Fig. 10 (a) Artistic impression of the experimental scheme for the HCN detection from *Pseudomonas* bacteria: air cylinder, high pressure cylinder of synthetic air; flow controllers, mechanical mass flow controllers; sample cuvette, glass cuvette with the sample to analyze; empty cuvette, empty glass for reference comparison; overpressure outlets, outlets to prevent overpressure inside cuvettes; needle valve, Teflon needle valve to reduce the pressure inside the PA cell; valves, diaphragm isolated three-way valves; incubator, environmental chamber set at 37°C; OPO, continuous wave optical parametric oscillator; PA cell, photoacoustic cell with Silcosteel coating. (b) Concentration dynamics of HCN emitted by *Pseudomonas* bacteria (red dots) with the data from the reference cuvette (black dots). Zero time corresponds to the bacteria inoculation. The maximum value of 6.5 ppmv was reached after 77 h (~3.2 days). New medium was added at 190 h (~7.9 days). After adding this new substrate HCN production started again after a lag phase of 10 h reaching peak of 2.1 ppmv.

1 ml of a McFarland standard with an optical density of 0.5 (at 600 nm) was inoculated in 50 ml of liquid BHI medium in a 250 ml Erlenmeyer flask adapted for the gas flow sampling; this resulted in an initial concentration of 2 to 5×10^{-6} colony-forming units (CFU)/ml. The Erlenmeyer flasks have glass stoppers fitted with two Teflon open/close valves acting as the inlet and outlet for gas sampling. Bacterial filters (FP 30/0.2Ca – S, Whatman GmbH, Germany) were placed on the inlet and outlet of the flasks to prevent contamination.[56] The bacteria were kept in an environmental chamber (Environmental Test Chamber, Sanyo, Japan) at 37°C and the headspace of the samples was constantly flushed with a mixture of 21% O_2 in nitrogen, controlled with mass flow controllers at a total flow rate of 3.4 L/h. From the headspace, a flow of 3 L/h was led to the photoacoustic cell. Overflow needle outlets were placed between the outlet of each cuvette and the selector valve to keep a constant air flow through the cuvette and to maintain a pressure inside the photoacoustic cell of 400 mbar. During the experiment, the cuvettes were constantly shaken at 70 rpm. A blank control measurement was provided by a cuvette containing only a medium with liquid BHI without *Pseudomonas* bacteria. In such a way, potential HCN background production by the medium could be investigated. These samples and reference cuvettes were monitored alternately. Figure 10(a) shows the artistic impression of the experimental setup; Fig. 10(b) shows the background HCN production by the medium (black dots) and *Pseudomonas* bacteria (red dots). Each datum point and its error bar represent the mean of the last 10 points of each measurement cycle. No HCN production could be observed for the blank sample containing only medium (<10 ppbv). At time $t = 0$, bacteria were inoculated in the medium. After 20 h, the bacteria start to produce exponentially HCN reaching concentrations as high as 6.5 ppmv after 77 h. Then the production ceases; this production decrease is most likely caused by depletion of the medium. Bacteria run out of substrate and therefore stop producing HCN. This hypothesis was confirmed by adding 20 ml new medium at 190 h (7.9 days), at which point HCN production started again after a lag phase of 10 h. However, absolute HCN production was not as high as at first time (2.1 ppmv in comparison with 6.5 ppmv), in which specific substances in the medium are limiting the HCN production will be subject to further investigations.

4 Conclusion

An OPO-based PAS was successfully tested for trace gas detection of HCN emission from clover leaves, human breath, and *Pseudomonas* bacteria. The OPO-based detection system showed a good detection stability over a period of 13 days. The latter is a great advantage when measuring long-term biomedical samples. The achieved detection limit for HCN was determined at 0.4 ppbv measured at 3287.25 cm^{-1} in 10 s, which is equivalent to an overall sensitivity of the system of $2.5 \times 10^{-9} cm^{-1} Hz^{-1/2}$. Future plans include monitoring the HCN production of different types of *Pseudomonas* bacteria under different environmental conditions. This research will also extend to the HCN detection in human exhaled breath and plant physiology experiments.

Acknowledgments

The authors would like to thank Cor Sikkens and Peter Claus (Radboud University Nijmegen, The Netherlands) for their technical help in these experiments. Furthermore, we would like to acknowledge the Microbiology Department at Radboud University Nijmegen Medical Centre (Nijmegen, The Netherlands) for providing their microbiological materials. The research was financially supported by the Long Fonds, (The Netherlands, Project No. 3.3.11.002), IOP Photonic devices, the Province of Gelderland and EFRO. Also M.P.P. Castro is grateful to thank Coordenação de Aperfeiçoamento de Pessoal de Nivel Superior—CAPES-Brazil for her scholarship at the Radboud University.

References

1. J. Taylor et al., "Toxicological profile for cyanide," http://www.atsdr.cdc.gov/toxprofiles/tp8-c1.pdf (2006).
2. F. M. Schmidt et al., "Background levels and diurnal variations of hydrogen cyanide in breath and emitted from skin," *J. Breath Res.* **5**(4), 1–10 (2011).
3. D. A. Jones, "Why are so many food plants cyanogenic?" *Phytochemistry* **47**(2), 155–162 (1998).
4. J. E. Tintinalli, G. D. Kelen, and J. S. Stapczynski, *Emergency Medicine: A Comprehensive Study Guide*, McGraw-Hill Professional, Blacklick, OH (2004).
5. I. Siegien and R. Bogatek, "Cyanide action in plants—from toxic to regulatory," *Acta Physiol.* **28**(5), 483–497 (2006).
6. G. D. Peiser et al., "Formation of cyanide from carbon-1 of 1-aminocyclopropane-1-carboxylic acid during its conversion to ethylene," *Proc. Natl. Acad. Sci. U. S. A.* **81**(10), 3059–3063 (1984).
7. J. M. Miller and E. E. Conn, "Metabolism of hydrogen-cyanide by higher-plants," *Plant Physiol.* **65**(6), 1199–1202 (1980).
8. K. Refsgaard et al., "Dissipation of cyanogenic glucosides and cyanide in soil amended with white clover (Trifolium repens L.)," *Soil Biol. Biochem.* **42**(7), 1108–1113 (2010).
9. M. A. Hughes and E. E. Conn, "Cyanoglucoside biosynthesis in white clover (Trifolium repens)," *Phytochemistry* **15**(5), 697–701 (1976).
10. A.-S. Blier et al., "Quantification of Pseudomonas aeruginosa hydrogen cyanide production by a polarographic approach," *J. Microbiol. Methods* **90**(1), 20–24 (2012).
11. W. Lenney and F. Gilchrist, "Pseudomonas aeruginosa and cyanide production," *Eur. Respir. J.* **37**(3), 482–483 (2011).
12. M. Rosenfeld et al., "Early pulmonary infection, inflammation, and clinical outcomes in infants with cystic fibrosis," *Pediatr. Pulmonol.* **32**(5), 356–366 (2001).
13. J. Emerson et al., "Pseudomonas aeruginosa and other predictors of mortality and morbidity in young children with cystic fibrosis," *Pediatr. Pulmonol.* **34**(2), 91–100 (2002).
14. P. M. Quinton, "Cystic fibrosis: a disease in electrolyte transport," *FASEB J.* **4**(10), 2709–2717 (1990).
15. S. H. Cheng et al., "Defective intracellular transport and processing of CFTR is the molecular basis of most cystic fibrosis," *Cell* **63**(4), 827–834 (1990).
16. G. M. Roomans, "Pharmacological treatment of the ion transport defect in cystic fibrosis," *Expert Opin. Invest. Drugs* **10**(1), 1–19 (2001).
17. R. C. Boucher, "Airway surface dehydration in cystic fibrosis: pathogenesis and therapy," *Annu. Rev. Med.* **58**, 157–170 (2007).
18. J. J. Smith et al., "Cystic fibrosis airway epithelia fail to kill bacteria because of abnormal airway surface fluid," *Cell* **85**(2), 229–236 (1996).
19. B. Frederiksen, C. Koch, and N. Hoiby, "Antibiotic treatment of initial colonization with Pseudomonas aeruginosa postpones chronic infection and prevents deterioration of pulmonary function in cystic fibrosis," *Pediatr. Pulmonol.* **23**(5), 330–335 (1997).
20. B. Enderby et al., "Hydrogen cyanide as a biomarker for Pseudomonas aeruginosa in the breath of children with cystic fibrosis," *Pediatr. Pulmonol.* **44**(2), 142–147 (2009).
21. M. D. Stutz et al., "Cyanide in bronchoalveolar lavage is not diagnostic for Pseudomonas aeruginosa in children with cystic fibrosis," *Eur. Respir. J.* **37**(3), 553–558 (2011).
22. S. U. Savelev et al., "Volatile biomarkers of Pseudomonas aeruginosa in cystic fibrosis and noncystic fibrosis bronchiectasis," *Lett. Appl. Microbiol.* **52**(6), 610–613 (2011).

23. M. M. Baum et al., "Hydrogen cyanide exhaust emissions from in-use motor vehicles," *Environ. Sci. Technol.* **41**(3), 857–862 (2007).
24. K. Stamyr et al., "Background levels of hydrogen cyanide in human breath measured by infrared cavity ring down spectroscopy," *Biomarkers* **14**(5), 285–291 (2009).
25. J. A. Ma and P. K. Dasgupta, "Recent developments in cyanide detection: a review," *Anal. Chem. Acta* **673**(2), 117–125 (2010).
26. J. Q. Ren, W. H. Zhu, and H. Tian, "A highly sensitive and selective chemosensor for cyanide," *Talanta* **75**(3), 760–764 (2008).
27. C. Mannel-Croise, B. Probst, and F. Zelder, "A straightforward method for the colorimetric detection of endogenous biological cyanide," *Anal. Chem.* **81**(22), 9493–9498 (2009).
28. W. C. Blackledge et al., "New facile method to measure cyanide in blood," *Anal. Chem.* **82**(10), 4216–4221 (2010).
29. S. Jermak, B. Pranaityte, and A. Padarauskas, "Headspace single-drop microextraction with in-drop derivatization and capillary electrophoretic determination for free cyanide analysis," *Electrophoresis* **27**(22), 4538–4544 (2006).
30. M. Tomasulo and F. M. Raymo, "Colorimetric detection of cyanide with a chromogenic oxazine," *Org. Lett.* **7**(21), 4633–4636 (2005).
31. C. Mannel-Croise and F. Zelder, "Side chains of cobalt corrinoids control the sensitivity and selectivity in the colorimetric detection of cyanide," *Inorg. Chem.* **48**(4), 1272–1274 (2009).
32. K. Papezova and Z. Glatz, "Determination of cyanide in microliter samples by capillary electrophoresis and in-capillary enzymatic reaction with rhodanese," *J. Chromatogr., A* **1120**(1–2), 268–272 (2006).
33. L. Meng et al., "Simultaneous derivatization and extraction of free cyanide in biological samples with home-made hollow fiber-protected headspace liquid-phase microextraction followed by capillary electrophoresis with UV detection," *J. Chromatogr., B* **877**(29), 3645–3651 (2009).
34. L. Shang and S. J. Dong, "Design of fluorescent assays for cyanide and hydrogen peroxide based on the inner filter effect of metal nanoparticles," *Anal. Chem.* **81**(4), 1465–1470 (2009).
35. J. Lv et al., "A micro-chemiluminescence determination of cyanide in whole blood," *Forensic Sci. Int.* **148**(1), 15–19 (2005).
36. A. Abbaspour et al., "A selective modified carbon paste electrode for determination of cyanide using tetra-3,4-pyridinoporphyrazinatocobalt(ii)," *Talanta* **66**(4), 931–936 (2005).
37. C. K. Zacharis et al., "Amperometric determination of cyanides at the low ppb level by automated preconcentration based on gas diffusion coupled to sequential injection analysis," *Talanta* **77**(5), 1620–1626 (2009).
38. P. Dumas, G. Gingras, and A. LeBlanc, "Isotope dilution-mass spectrometry determination of blood cyanide by headspace gas chromatography," *J. Anal. Toxicol.* **29**(1), 71–75 (2005).
39. I. Lindsay et al., "110 GHz rapid, continuous tuning from an optical parametric oscillator pumped by a fiber-amplified DBR diode laser," *Opt. Express* **13**(4), 1234–1239 (2005).
40. A. K. Y. Ngai et al., "Automatically tunable continuous-wave optical parametric oscillator for high-resolution spectroscopy and sensitive trace-gas detection," *Appl. Phys. B* **85**(2–3), 173–180 (2006).
41. A. K. Y. Ngai et al., "Continuous wave optical parametric oscillator for quartz-enhanced photoacoustic trace gas sensing," *Appl. Phys. B* **89**(1), 123–128 (2007).
42. B. Hardy et al., "Compact, single-frequency, doubly resonant optical parametric oscillator pumped in an achromatic phase-adapted double-pass geometry," *Opt. Lett.* **36**(5), 678–680 (2011).
43. M. Sigrist et al., "Environmental applications of laser-based photoacoustic spectroscopy," *Anal. Sci.* **17**(S1), S511–S514 (2001).
44. V. Koskinen et al., "Extremely sensitive trace gas analysis with modern photoacoustic spectroscopy," *Vib. Spectrosc.* **42**(2), 239–242 (2006).
45. S. M. Cristescu et al., "Laser-based systems for trace gas detection in life sciences," *Appl. Phys. B* **92**(3), 343–349 (2008).
46. D. D. Arslanov et al., "Real-time, subsecond, multicomponent breath analysis by optical parametric oscillator based off-axis integrated cavity output spectroscopy," *Opt. Express* **19**(24), 24078–24089 (2011).
47. M. W. Sigrist et al., "Trace gas monitoring with infrared laser-based detection schemes," *Appl. Phys. B* **90**(2), 289–300 (2008).
48. C. Wang and P. Sahay, "Breath analysis using laser spectroscopic techniques: breath biomarkers, spectral finger-prints, and detection limits," *Sensors* **9**(10), 8230–8262 (2009).
49. A. Miklos and P. Hess, "Application of acoustic resonators in photoacoustic trace gas analysis and metrology," *Rev. Sci. Instrum.* **72**(4), 1937–1955 (2001).
50. M. W. Sigrist, "Trace gas monitoring by laser photoacoustic spectroscopy and related techniques plenary," *Rev. Sci. Instrum.* **74**(1), 486–490 (2003).
51. M. van Herpen et al., "Tuning and stability of a continuous-wave mid-infrared high-power single resonant optical parametric oscillator," *Appl. Phys. B* **75**(2–3), 329–333 (2002).
52. D. D. Arslanov et al., "Continuous-wave optical parametric oscillator based infrared spectroscopy for sensitive molecular gas sensing," *Laser Photonics Rev.* **7**(2), 188–206 (2013).
53. L. Rothman et al., "The HITRAN 2008 molecular spectroscopic database," *J. Quant. Spectrosc. Radiat. Transfer* **110**(9–10), 533–572 (2009).
54. H.-P. Loock and P. D. Wentzell, "Detection limits of chemical sensors: applications and misapplications," *Sens. Actuators, B* **173**, 157–163 (2012).
55. T. H. Risby and F. K. Tittel, "Current status of midinfrared quantum and interband cascade lasers for clinical breath analysis," *Opt. Eng.* **49**(11), 111123 (2010).
56. E. Crespo et al., "Proton transfer reaction mass spectrometry detects rapid changes in volatile metabolite emission by Mycobacterium smegmatis after the addition of specific antimicrobial agents," *J. Microbiol. Methods* **86**(1), 8–15 (2011).